Measurements and Analysis of Angular Distributions and Anisotropy of Fission Fragments from Neutron-Induced Fission of ^{232}Th, ^{233}U, ^{235}U, ^{238}U, ^{239}Pu, ^{237}Np, ^{nat}Pb and ^{209}Bi in Intermediate Energy Range 1–200 MeV

A.S. Vorobyev[1], A.M. Gagarski[1], O.A. Shcherbakov[1], L.A. Vaishnene[1], A.L. Barabanov[2,3]

[1]*NRC "Kurchatov Institute", B.P. Konstantinov Petersburg Nuclear Physics Institute, 188300, Gatchina, Leningrad district, Russia*
[2]*NRC "Kurchatov Institute", 123182, Moscow, Russia*
[3]*Moscow Institute of Physics and Technology, 141700, Dolgoprudny, Moscow Region, Russia*

Abstract

Angular distributions of fission fragments from the neutron-induced fission of ^{232}Th, ^{233}U, ^{235}U, ^{238}U, ^{239}Pu, ^{237}Np, ^{nat}Pb and ^{209}Bi have been measured in the energy range 1–200 MeV at the neutron TOF spectrometer GNEIS based on the spallation neutron source at 1 GeV proton synchrocyclotron SC-1000 of the NRC KI - PNPI (Gatchina, Russia). The data in the neutron energy range above 20 MeV for ^{233}U, ^{239}Pu, ^{237}Np, ^{nat}Pb and ^{209}Bi have been obtained for the first time. Recently, the list of nuclei to be studied within the framework of present investigation was filled with isotope ^{237}Np. Neptunium is a major component of spent nuclear fuel, therefore an accurate knowledge of the fission cross-section and fragment properties is needed for waste transmutation and advanced nuclear facilities (reactors, ADS, etc.) studies. A description of the experimental equipment and measurement procedure is given. The underlying ideas of the theoretical approach developed for analysis of the obtained experimental data are discussed.

1. Introduction

The experimental study of angular distributions of fission fragments near the threshold and low chance fission is a way to determine the properties of transition states of fissioning nucleus at the saddle point. The information about angular distribution of fission fragment is also very important to verify parameters of theoretical models used for adequate fission process description in neutron energy range above 20 MeV. The data on nuclear fission in intermediate energy range 1–200 MeV are of prime importance for the advanced nuclear technologies such as Accelerator-Driven Systems (for nuclear power generation and nuclear transmutation). The systematic study of angular distributions of fission fragments is limited to that these experimental data are very scarce in neutron energy range above 20 MeV and are practically absent for neutron energy range above 100 MeV.

In this report, we summarize the results of the measurements carried out at the neutron time-of-flight (TOF) spectrometer GNEIS of the NRC KI - PNPI during the last few years. The main features of the experimental set-up are also described. To demonstrate the quality of obtained data, the comparison with the results obtained by other experimental groups is performed. The data obtained in recent measurement for the reaction ^{237}Np(n,f) are also shown. Besides, we present a method for calculation of fission fragment angular distribution and compare the results of calculations with the experimental data for ^{237}Np nucleus.

2. General description of the experiment

The measurements were carried out at the 36 m flight path of the neutron TOF-spectrometer GNEIS based on the spallation neutron source at 1 GeV proton synchrocyclotron SC-1000 of the NRC KI - PNPI (Gatchina, Russia) [1, 2]. The short pulse width 10 ns of the neutron source enables to carry out TOF-measurements with the energy resolution from 0.8% (at 1 MeV) to 13% (at 200 MeV). A schematic view of the experimental set-up is shown in Fig. 1. The main features of the measurements are described below. A detailed description of the set-up can be found in our previous publications [3–10].
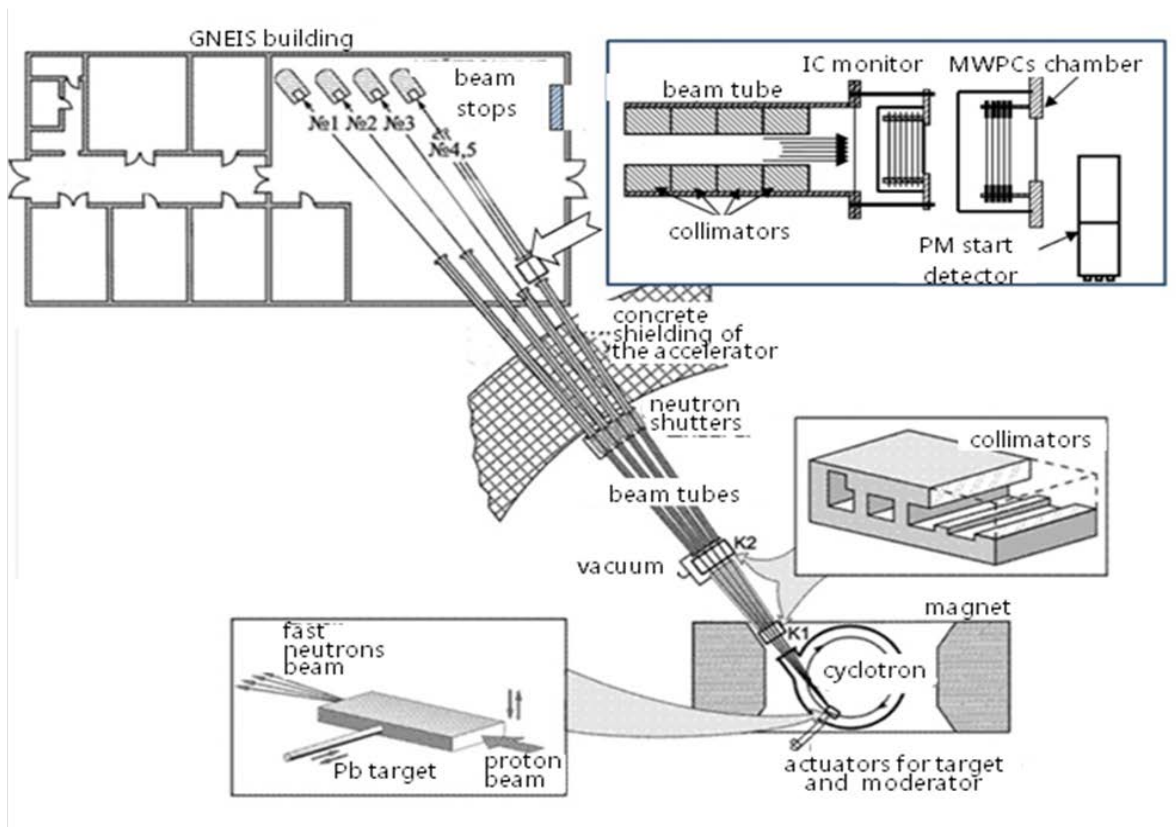

Fig. 1. Schematic view of the experimental set-up.

The measurements of angular distributions of fission fragments (FF) were carried out using the FF detector which consists of two low pressure gaseous coordinate-sensitive multiwire proportional counters D1 and D2 (MWPC, see in upper right corner of Fig. 1). The counters D1 and D2 were placed close to the target in the beam, one after the other. The neutron beam axis came through the geometrical centers of the target and the MWPC's electrodes being perpendicular to them. Data acquisition system was based on two waveform digitizers Acqiris DC-270 with sampling rate of 500 MSamples/s. This system as well as the methods of digital processing of signals from FF detector used enabled to perform measurements in a wide interval of neutron energy with a zero dead time. Herewith, almost perfect separation between fission events and products of other reactions was achieved at a practically zero FF registration threshold. To demonstrate the quality of this separation, for ^{237}Np measurements the two-dimensional plots of the amplitudes of correlated cathode signals from two MWPCs are shown in Fig. 2 for all events and for "useful" fission events (left part and right part, respectively) selected by means of the procedure described in [4].
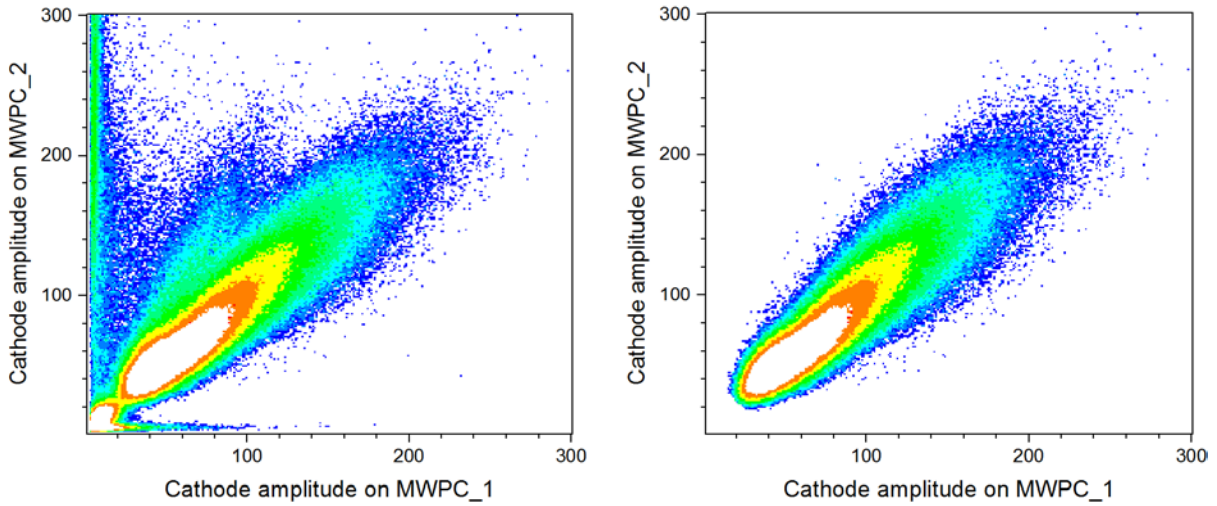
Fig. 2. A two-dimensional plot of the amplitudes of the cathode signals from two MWPCs in ^{237}Np experiment. Right part of this figure shows only "useful" fission events.

The measured angular distributions for selected fission fragment events were corrected for the efficiency of fission fragment registration. This efficiency was calculated by means of the Monte-Carlo method taking into account the real geometry, design and features of the fission fragment detector.

Note that the effect of momentum transfer from the incident neutron to the fissioning system on the angular distributions in the laboratory system should be taken into account. To determine this effect, angular distributions of fission fragments in the laboratory system were measured for two set-up orientations relative to the beam direction (downstream and upstream). In the first, downstream, position, the beam direction coincides with the longitudinal momentum component of the detected fission fragment. In the second, upstream, position, the beam direction is opposite to the longitudinal momentum component of the detected fission fragment.

The angular distributions of fission fragments in the center-of-mass system were deduced from the corrected $\cos(\theta)$ angular distributions in the laboratory system for two set-up orientations relative to the neutron beam direction ($\cos(\theta)$ bins were equal to 0.01). Then, these distributions were fitted in the range $0.24 < \cos(\theta) < 1.0$ by the sum of even Legendre polynomials up to the 4-th order and their anisotropy $W(0°)/W(90°)$ was calculated using the coefficients A_2 and A_4 ($A_0=1$) for the corresponding Legendre polynomials:

$$\frac{W(0°)}{W(90°)} = \frac{1 + A_2 + A_4}{1 - A_2/2 + 3A_4/8}. \tag{1}$$

3. Results and discussion

The experimental data on angular distributions of fission fragments in the neutron-induced fission have been accumulated over decades, mostly for neutron energy less than 20 MeV. A new age in experimental investigations of the fission fragment angular distributions started when new experiments dedicated to this problem have been initiated nearly simultaneously by the GNEIS team at NRC KI - PNPI [3–11], the n_TOF Collaboration at CERN [12–16], and the NIFFTE Collaboration in Los Alamos [17, 18]. The

pulsed high-intensity "spallation" neutron sources of these facilities enable to carry out TOF-measurements of the neutron-induced fission cross sections and fission fragment angular distributions in intermediate neutron energy range 1–300 MeV. The other two principally important features of the experimental techniques employed by these research groups are usage of the multichannel position-sensitive detectors of fission fragments of different degree of complexity (MWPCs, PPACs, TPC), and application of the waveform digitizers for detector pulse processing. The results of these investigations are presented in Table 1.

Table 1. Status of experiments on angular distributions of fission fragment study.

Nucleus	GNEIS, KI-PNPI	n-TOF, CERN	LANSCE, LANL	TSL, Uppsala University
	Reference, EXFOR [19] Accession #			
^{232}Th	[3, 6, 10]- #41608	[12, 13], [14]- #23209		[20]- #22898
^{233}U	[4, 8, 10]- #41616			
^{235}U	[3, 6, 10]- #41608	[15, 16]	[17, 18]	
^{238}U	[3, 6, 10]- #41608	[15]		[20]- #22898
^{237}Np	[11]			
^{239}Pu	[5, 9]- #41658			
^{nat}Pb	[5, 9]- #41658			
^{209}Bi	[4, 8, 10]- #41616			

It is seen that a large amount of new data has been obtained recently at the TOF spectrometer GNEIS. Comparison of angular distributions of fission fragments obtained in this work and literature data in neutron energy range less 20 MeV demonstrates that there is a good agreement between all experimental data. For example, Fig. 3 shows the angular distributions of fission fragments in the center-of-mass system for ^{233}U and ^{239}Pu for two neutron energy intervals, 1.49±0.16 MeV (left part of Fig. 3) and 15.7±1.4 MeV (right part of Fig. 3) in comparison with experimental data of other authors [21–25]. The results of the data fitting by the sum of even Legendre polynomials up to the 4th order are also shown in Fig. 3. It should be noted that experimental techniques used by referred authors differ both in fragment detectors and in neutron sources. It may be interpreted as a convincing proof of accuracy and reliability of our measurement technique and data handling procedure, at least in the neutron energy range below 20 MeV.

The reliability of the experimental set-up and data processing applied in this work is confirmed by the fact that the obtained energy dependence of anisotropy is the same as in the other works (see [3–11]). It can be stated that the results obtained at the GNEIS below ~ 20 MeV adequately represent the structures in energy behavior of the anisotropy observed in early measurements. A comparison of our results obtained in the neutron energy range 20–200 MeV with the latest data measured by NEFFTE and n_TOF collaborations demonstrates a good agreement between these data within experimental uncertainties.
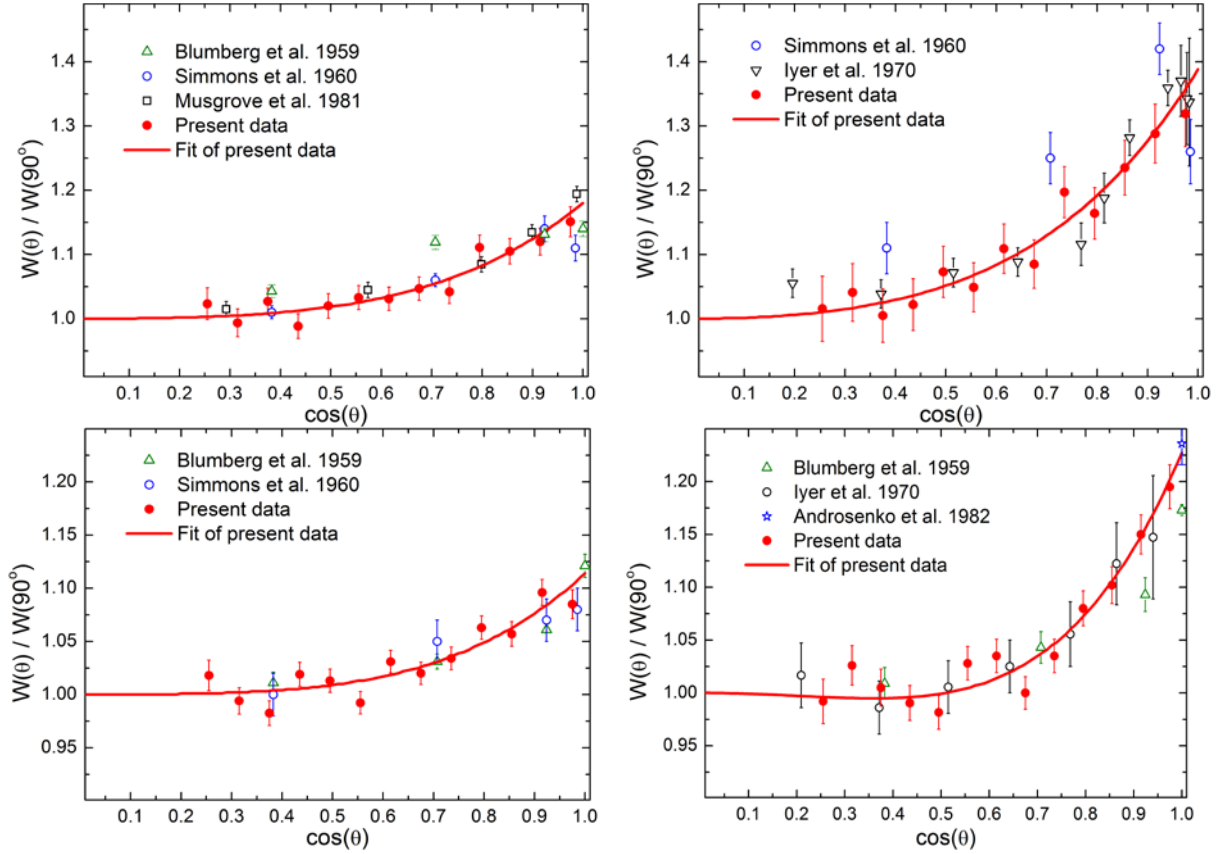
Fig. 3. Example of angular distributions for ^{233}U(n,f) – upper part and ^{239}Pu(n,f) – lower part. The error bars represent statistical uncertainties. Solid line is a result of the fitting by the sum of even Legendre polynomials up to the 4th order.

The anisotropy of the angular distribution of fragments is a consequence of the spin orientation of the fissioning nucleus, which arises due to the orbital momentum of incident neutrons is perpendicular to the direction of their motion (z axis). The angular distribution of fragments from fission of the nucleus with spin J and parity π is described by the formulas

$$\frac{dw^{J\pi}(\theta)}{d\Omega} = \sum_M \eta^{J\pi}(M) \sum_K \rho^{J\pi}(K) \frac{dw^J_{MK}(\theta)}{d\Omega}, \quad dw^J_{MK}(\theta) = \frac{2J+1}{4\pi} |d^J_{MK}(\theta)|^2 \, d\Omega. \quad (1)$$

The diagonal elements of spin density matrix $\eta^{J\pi}(M)$ and the quantities $\rho^{J\pi}(K)$ determine the probability distributions over projections M and K of spin J on the axis z and the nuclear deformation axis, respectively. The distribution over K is defined by the fission mechanism as well as by the shape of the nucleus at the saddle point; here $\rho^{J\pi}(K) = \rho^{J\pi}(-K)$, if we neglect the very small effects of parity violation. The spin orientation can also be given by irreducible components of the density matrix or, in other words, by the orientation spin-tensors

$$\tau_{Q0}(J\pi) = \sum_M C^{JM}_{JMQ0} \eta^{J\pi}(M), \quad (2)$$

where C^{Aa}_{BbDd} are Clebsch-Gordan coefficients.

Expressions (2) can be conveniently converted to the following form

$$\frac{dw^{J\pi}(\theta)}{d\Omega} = \frac{1}{4\pi}\sum_{Q} (2Q+1)\tau_{Q0}(J\pi)\beta_Q(J\pi)P_Q(\cos\theta),\tag{3}$$

where the anisotropy parameters are defined by the formula

$$\beta_Q(J\pi) = \sum_{K} C^{JK}_{JKQ0}\rho^{J\pi}(K),\tag{4}$$

and $P_Q(\cos\theta)$ are the Legendre polynomials. Summation is carried out only over even values of Q due to $\rho^{J\pi}(K) = \rho^{J\pi}(-K)$. If the distribution $\rho^{J\pi}(K)$ ($\eta^{J\pi}(M)$) is smooth, then the parameters $\beta_Q(J\pi)$ (the spin-tensors $\tau_{Q0}(J\pi)$) decrease rapidly with an increase of Q.

In neutron-induced reaction, an arising compound nucleus decays either into a particle and residual nucleus (generally, excited) or into two fragments. Another possibility is that after the collision, some particle and some residual nucleus are formed as a result of a direct or pre-equilibrium process (we neglect the output channels with three or more particles). We assume for simplicity that all excited residual nuclei are in equilibrium compound states and, consequently, their further decay (into a particle and a new residual nucleus or into two fragments) is described by the statistical model (as the decay of the primary compound nucleus). Let the index i numerates the levels of a nucleus (with Z protons and N neutrons) with the same spin J and parity π, $\sigma_{ZN}(J\pi i)$ is the population cross section of the corresponding level, and $P_f^{ZN}(J\pi i)$ is the fission probability for the nucleus on this level. Thus, the observed fission cross section is determined by

$$\sigma_f = \sum_{ZNJ\pi i} \sigma_{ZN}(J\pi i)P_f^{ZN}(J\pi i),\tag{5}$$

where summation over i is an integration if the levels lie in the continuum. Clearly, each cross section $\sigma_{ZN}(J\pi i)$ is a sum of population cross sections $\sigma_{ZN}(J\pi iM)$ of states (J,π,i) with definite spin projection M on the axis z (then $\eta_{ZN}^{J\pi i}(M) = \sigma_{ZN}(J\pi iM)/\sigma_{ZN}(J\pi i)$), while the probability $P_f^{ZN}(J\pi i)$ is a sum of probabilities of fission $P_f^{ZN}(J\pi iK)$ via transition states with projection K of spin on the deformation axis (then $\rho_{ZN}^{J\pi}(K) = P_f^{ZN}(J\pi iK)/P_f^{ZN}(J\pi i)$). Therefore, the observed differential fission cross section takes the form

$$\frac{d\sigma_f(\theta)}{d\Omega} = \sum_{ZNJ\pi i} \sigma_{ZN}(J\pi i)P_f^{ZN}(J\pi i)\frac{dw_{ZN}^{J\pi i}(\theta)}{d\Omega} = \frac{1}{4\pi}\sum_{Q=0,2,4,\dots} \sigma_{fQ}P_Q(\cos\theta),\tag{6}$$

where

$$\sigma_{fQ} = (2Q+1)\sum_{ZNJ\pi i} \sigma_{ZN}(J\pi i)P_f^{ZN}(J\pi i)\tau_{Q0}^{ZN}(J\pi i)\beta_Q^{ZN}(J\pi i),\tag{7}$$

and $\sigma_{f0} = \sigma_f$.

Thus, the observed fission fragment angular distribution

$$W(\theta) \equiv \frac{1}{\sigma_f} \frac{d\sigma_f(\theta)}{d\Omega} = \frac{1}{4\pi} \left(1 + \sum_{Q=2,4,\ldots} A_Q P_Q(\cos\theta) \right) \qquad (8)$$

is a series over Legendre polynomials. Since, in practice, at least one of the distributions over M or over K is smooth, the coefficients A_Q rapidly decrease with increasing of Q, so that with rare exceptions, the shape of the angular distribution is determined by a single parameter A_2. This parameter can be derived from angular anisotropy $W(0°)/W(90°)$. But even if A_4 is significantly different from zero (but always significantly less than A_2), the results of measurements of angular distributions of fragments are usually recalculated into anisotropy by the formula (1).

Earlier, only in the work [20] an appropriate attempt was made to describe the angular distribution of fragments in nuclear fission by neutrons in a wide range of energies, up to 100 MeV. The results of the calculations were compared with the experimental data on ^{232}Th and ^{238}U target nuclei presented in the same work. However, there were no further publications by these authors, which would have provided the necessary details about the method used or performed calculations for other target nuclei.

We made simplifications in the calculation scheme using the following qualitative considerations. The spin $\vec{J} = \vec{s} + \vec{I} + \vec{l}$ of the compound nucleus consists of the spins of the incident particle s, the target nucleus I, and the relative orbital momentum l. If s and I are not oriented, then the spin J is directed primarily across the axis z. At high energies l (and J) is large, so that the spin orientation of the compound core is very noticeable. At the same time, the particles emitted during the statistical decay of the compound nucleus have relatively low energies, of the order of nuclear temperature, and, consequently, carry away small angular momenta. Therefore, the orientation of the residual core remains noticeable. If there is a direct or pre-equilibrium process, the particles are usually emitted with high energies and, consequently, with large angular momenta. Therefore, there is no reason to expect that the residual nuclei will have a noticeable spin orientation. Therefore, we have identified two components in the total fission cross section, σ_f^{DPE} and σ_f^{C}. The first one is due to the fission of residual nuclei, the formation of which was preceded by a direct (D) or preequilibrium (PE) process, while the second contribution (C) is due to the fission of the compound nucleus and the residual nuclei formed at some stage of statistical decay of the primary compound nucleus. Assuming the DPE component of the differential fission cross section is completely isotropic, instead of (7), (8) we get

$$\frac{d\sigma_f(\theta)}{d\Omega} = \frac{\sigma_f}{4\pi} + \frac{1}{4\pi} \sum_{Q=2,4,\ldots} \sigma_{fQ}^C P_Q(\cos\theta), \qquad (9)$$

where the quantities

$$\sigma_{fQ}^C = (2Q+1) \sum_{ZNJ\pi i} \sigma_{ZN}^C(J\pi i) P_f^{ZN}(J\pi i) \tau_{Q0}^{CZN}(J\pi i) \beta_Q^{ZN}(J\pi i) \qquad (10)$$

are determined by the population cross sections $\sigma_{ZN}^C(J\pi i)$ and the orientation spin-tensors $\tau_{Q0}^{CZN}(J\pi i)$ of the levels, which belong either to the primary compound nucleus or to the residual nuclei formed in the statistical decay of this compound nucleus.

The details of the calculation of the anisotropy parameters (5) are given in the article [11]. Here we only point out that above the barrier we use a statistical distribution, $\rho_{ZN}^{J\pi i}(K) \sim e^{-K^2/2K_0^2}$, where the parameter $K_0^2 = J_{\text{eff}}T/\hbar^2$ is determined by the nuclear temperature T on the barrier and the effective moment of inertia J_{eff}, while below the barrier we take $\rho_{ZN}^{J\pi i}(K) \sim e^{-\alpha(|K|-K_1)^2}$, where α is a fixed parameter, and K_1 is the spin projection for the dominant transition state. In the region of intermediate collision energies, fissioning nuclei tend to have sufficiently high excitation energies, so that the shape of distribution over K for energies below the barrier is insignificant for most isotopes. Only in the region of very low collision energies, when the fission of the compound nucleus ^{238}Np is sub-barrier, the value of K_1 for the isotope ^{238}Np determines the type of angular distribution of the fragments; the choice of K_1 for the isotope ^{237}Np in the region of the threshold energy for the reaction $(n,n'f)$ is also significant. We have considered the parameter K_1 as adjustable only for ^{238}Np, but K_1 was assumed to be 0.5 for ^{237}Np and 1.5 for all other isotopes.
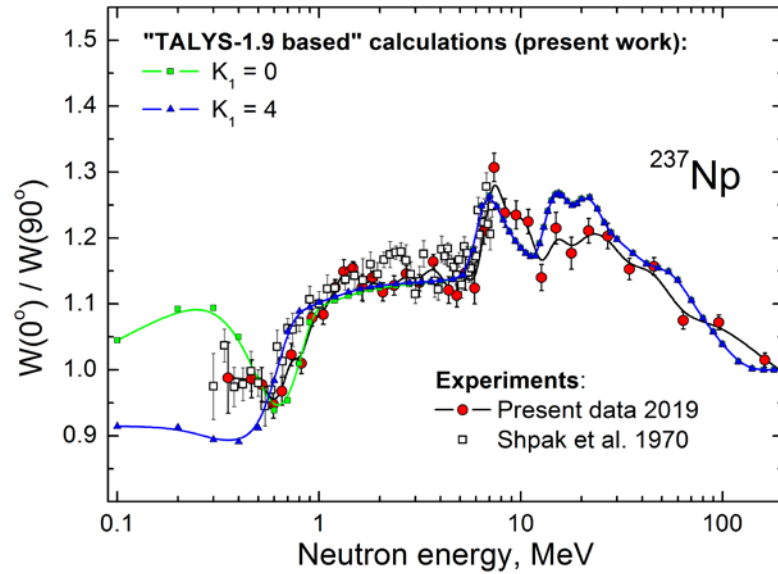

Fig. 4. Anisotropy of fission fragments of ^{237}Np. Points with error bars – experimental data. Lines with symbols – calculation performed using the proposed method with K_1 equals to 0 and 4 for ^{238}Np.

There are a lot of computer codes that simulate collisions of particles with nuclei at energies from low to intermediate; the multi-purpose complex TALYS [26] is one of them. However, the angular distributions of fission fragments cannot be calculated either in TALYS or in other similar programs, even at low energies, as well as at the entire intermediate region up to 200 MeV. We made the additions to the TALYS program to calculate the orientation spin-tensors of nuclear states and the anisotropy parameters. Thus, we obtained a tool for calculating the angular distributions of fragments. The results obtained for the reaction ^{237}Np(n,f) are shown in Fig. 4 together with our experimental data and values of the anisotropy from Ref. [27]. There is a good agreement between the experiment and model calculation.

4. Conclusion

The purpose of our research is to obtain new experimental data on the angular distributions of fission fragments for different target nuclei in the neutron energy range from 1 to 200 MeV, as well as to develop theoretical models and computer codes describing experimental distributions. In this paper we presented the results of recent measurements for the reaction ^{237}Np(n,f) as well of the calculations for the same reaction. For the entire specified energy range, such results are obtained and demonstrated for the first time. We used a modified software package TALYS. At this initial stage of the work with this code, simplifications were introduced to the model to minimize the number of additional parameters, in addition to those used in TALYS. So, for example, for all fissioning nuclei at all excitation energies, one value of the effective moment of inertia was used, obviously, this is some average value. With a reasonable value of this parameter, the calculated curve describes the gross structure of the energy dependence of the angular anisotropy of the fragments in the whole energy range of 0.5–200 MeV. An agreement of the calculated values of the angular anisotropy of fission fragments with the measured ones is also due to taking into account the connection between the formation of angular anisotropy and compound nuclei decays. This allowed us to relate the decrease in the angular anisotropy in the region of neutron energies above 20–30 MeV with increase of the contributions of pre-equilibrium reactions. These results indicate both the appropriateness of our approach and the prospects for its further improvement in order to obtain new, more detailed information about characteristics of nuclei on barriers, as well as the role of preequilibrium processes in the interaction of nuclei with neutrons. Our next goal is the measurement and analysis of the fission fragment angular distributions for ^{240}Pu. The only two data sets for this nucleus were obtained earlier [28, 29]. An upper neutron energy range of these data does not exceed 10 MeV.

Acknowledgments

References

1. N.K. Abrosimov, G.Z. Borukhovich, A.B. Laptev, V.V. Marchenkov, G.A. Petrov, O.A. Shcherbakov, Yu.V. Tuboltsev, V.I. Yurchenko. Nucl. Instrum. Methods Phys. Res. A **242**, 121 (1985).
2. O.A. Shcherbakov, A.S. Vorobyev, E.M. Ivanov. Phys. Part. Nucl. **49**, 81 (2018).
3. A.S. Vorobyev, A.M. Gagarski, O.A. Shcherbakov, L.A. Vaishnene, A.L. Barabanov. JETP Letters **102**(**4**), 203 (2015).
4. A.S. Vorobyev, A.M. Gagarski, O.A. Shcherbakov, L.A. Vaishnene, A.L. Barabanov. JETP Letters **104**(**6**), 365 (2016).
5. A.S. Vorobyev, A.M. Gagarski, O.A. Shcherbakov, L.A. Vaishnene, A.L. Barabanov. JETP Letters **107**(**9**), 521 (2018).
6. A.M. Gagarski, A.S. Vorobyev, O.A. Shcherbakov, L.A. Vaishnene. In: "XXIII International Seminar on Interaction of Neutrons with Nuclei", Dubna, May 25–29, 2015. JINR, E3-2016-12, 2016, p.73.

7. A.M. Gagarski, A.S. Vorobyev, O.A. Shcherbakov, L.A. Vaishnene. In: "XXIV International Seminar on Interaction of Neutrons with Nuclei", Dubna, May 24–27, 2016. JINR, E3-2017-8, 2017, p.343.

8. A.S. Vorobyev, A.M. Gagarski, O.A. Shcherbakov, L.A. Vaishnene, A.L. Barabanov. In: "XXIV International Seminar on Interaction of Neutrons with Nuclei", Dubna, May 24–27, 2016. JINR, E3-2017-8, 2017, p.413.

9. A.M. Gagarski, A.S. Vorobyev, O.A. Shcherbakov, L.A. Vaishnene, A.L. Barabanov. In: "XXV International Seminar on Interaction of Neutrons with Nuclei", Dubna, May 22–26, 2017. JINR, E3-2018-12, 2018, p.342.

10. A.S. Vorobyev, A.M. Gagarski, O.A. Shcherbakov, L.A. Vaishnene, A.L. Barabanov. Proc. of the Int. Conf. "Nuclear data for Science and Technology ND-2016", September 11–16, 2016, Bruges, Belgium. EPJ Web of Conferences **146**, 04011 (2017).

11. A.S. Vorobyev, A.M. Gagarski, O.A. Shcherbakov, L.A. Vaishnene, A.L. Barabanov. JETP Letters **110**(**4**), 242 (2019).

12. L.S. Leong. PhD Thesis, Universite Paris Sud, CERN-Thesis-2013-254.

13. L.S. Leong, L. Tassan-Got, D. Tarrio, et al. Proc. of the Int. Conf. "Nuclear data for Science and Technology ND-2013", March 4–8, 2013, New York, USA. EPJ Web of Conferences **62**, 08003 (2013).

14. D. Tarrio, L.S. Leong, L. Audouin et al. Nuclear Data Sheets, **119**, 35 (2014).

15. E. Leal-Cidoncha, I. Duran, C. Paradela, et al. Proc. of "4th International Workshop on Nuclear Data Evaluation for Reactor applications WONDER-2015", October 5–8, 2015, Aix-en-Provence, France. EPJ Web of Conferences **111**, 10002 (2016).

16. E. Leal-Cidoncha, et al. FIESTA 2017, LANL FIESTA Fission School & Workshop, Santa Fe, 17–22 September 2017. https://t2.lanl.gov/fiesta2017/Talks/Leal-Cidoncha.pdf

17. V. Kleinrath. PhD Thesis, Technischen Universitat Wien, 2015.

18. V. Geppert-Kleinrath, F. Tovesson, J.S. Barrett et al. (NIFFTE Collaboration), Phys. Rev. C **99**, 064619 (2019).

19. V.V. Zerkin, B. Pritychenko. Nuclear Instruments and Methods. 2018. V. **888**. P. 31. http://www.nndc.bnl.gov/exfor

20. I.V. Ryzhov, M.S. Onegin, G.A. Tutin, J. Blomgren, N. Olsson, A.V. Prokofiev, P.-U. Renberg. Nucl. Phys. A **760**, 19 (2005).

21. J.E. Simmons, R.L. Henkel. Phys. Rev. **120**, 198 (1960).

22. R.H. Iyer, M.L. Sagu. Proc. of the Nuclear Physics and Solid State Physics Symposium, Dec. 27–30, 1970; Madurai, India: Nuclear Physics, Vol. **2**, p.57 (1970).

23. A.R. Musgrove, J.W. Boldeman, J.L. Cook, D.W. Lang, E.K. Rose, R.L. Walsh, J. Caruana, J.N. Mathur. J. Phys. G: Nucl. Phys. **7**, 549 (1981).

24. L. Blumberg, R.B. Leachman. Phys. Rev. **116**, 102 (1959).

25. Kh.D. Androsenko, G.G. Korolev, D.L. Shpak. VANT, Ser. Yadernye Konstanty **46**(**2**), 9 (1982).

26. A.J. Koning, S. Hilaire, M.C. Duijvestijn. "TALYS-1.0", Proc. Int. Conf. on Nuclear Data for Science and Technology (Nice, France, 2007), ed. by O. Bersillon, F. Gunsing, E. Bauge, R. Jacqmin, and S. Leray, EDP Sciences (2008), p.211.

27. D.L. Shpak, B.I. Fursov, G.N. Smirenkin. Sov. J. of Nucl. Physics **12**, 19 (1971).

28. Kh.D. Androsenko, G.N. Smirenkin. Sov. J. of Nucl. Physics **12**, 142 (1971).

29. J.E. Simmons, R.B. Perkins, R.L. Henkel. Phys. Rev. **137**, B809 (1965).